

Design, Optimization and CFD Simulation of a Nozzle for Industrial Cleaning Processes based on High-Pressure Water Jets

Shuce Zhang¹, Xueheng Tao^{1,2,3}, Jinshi Lu^{1,2}, Xuejun Wang^{1,2}, Zhenhua Zeng⁴

Abstract: Three different kinds of nozzles, normally used in industrial processes for the cleaning of material surface by means of water jets at high pressure (a Cylindrical Contracting, a Taper Contracting and Stepped nozzle), are numerically simulated with the express intent to optimize the related efficiency (cleaning effectiveness). Although some of them are found to display interesting properties, simulation results indicate that a helix nozzle displays the best jetting performances. It is shown that, as compared to improvements obtained by simply changing the jetting angle, revolving the fluid released from the helix nozzle can be used to create a grinding wheel on the cleaning surface, exerting a significant shearing action on the material to be cleaned.

Keywords: high pressure; water jet; cleaning; numerical simulation; nozzle structure optimization

1 Introduction

In the process of material surface cleaning by high pressure water jet, the enhancement of cleaning effectiveness and reduction of energy consumption have been significant areas of research for quite some time. Nurick (1976) studied the cavitation characteristics of sharp-edged orifices including circular orifices and rectangular orifices, and their effect on spray mixing (Nurick, 1976). Hashish and duPlessis (1978) developed a theory based on a control volume analysis, which

¹ School of Mechanical Engineering and Automation, Dalian Polytechnic University, Dalian, China, 116034

² National Engineering Research Center of Seafood, Dalian, China, 116034

³ Corresponding author, Ph.D, Professor. *E-mail address:* xhtao@dlpu.edu.cn

⁴ Dalian Modern Auxiliary Machines Development and Manufacturing Co. Ltd, Dalian, China, 116600

presented a basic method for building cutting equations to evaluate hydrodynamic forces (Hashish and duPlessis, 1978). Hitoshi (1996) focused on a peculiar phenomena occurring around high-speed submerged water jets, clarified the effectiveness of the nozzle structure and injection pressure therein, and then discussed the observed characteristics and configuration of the water jet (Hitoshi, 1996). A clear relationship between parameters (standoff distance and installation angle) and cleaning results was drawn by Gao and Chen (2006).

Keeping pump pressure constant and increasing jet velocity is a straightforward, economic method for optimizing a high pressure water jet cleaning device. This study, which focuses on nozzle configuration, posits a new nozzle and verifies its highly effective jet velocity by numerical simulation. Three kinds of nozzles commonly used in industrial production, the Cylindrical Contracting (CC) nozzle, Taper Contracting (TC) nozzle and Stepped nozzle, are simulated by FLUENT to obtain exact jet velocity comparison data. The most applicable of these is then sequentially optimized by simulating tentative structure design models. For the sequential optimization, a 3D model is used to simulate the helix nozzle outlet structure. Comparison results from the simulation of different nozzle inner surface configurations indicate the most favorable, best performing nozzle structure.

2 Preliminary optimization of nozzle structure

The nozzle structure determines the water jet velocity, which also determines the cleaning process. The Cylindrical Contracting (CC) nozzle, Taper Contracting (TC) nozzle and Stepped nozzle are those generally used in the industry currently. Figure 1 details their respective structures. The type of water jet that issues from all these different orifice nozzles has similar jet structures in air. Yanaida, Ohashi first detailed a geometrical description of the water jet in 1980 (Yanaida and Ohashi, 1980).

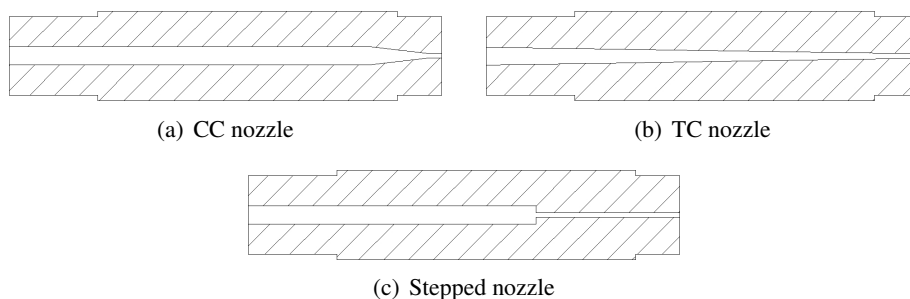


Figure 1: Nozzle structures

Over the past 40 years, a recognizable characteristic pattern has emerged. Jet structure, based on theory and observation, is shown in Figure 2 (Leu, Meng, Geskin and Tismeneskiy, 1998). The jet velocity equally distributes at the nozzle, but produces a considerable velocity difference as soon as it leaves the nozzle, compared to the boundary layer formed by the environment medium. The process of exchanging momentum and mass of jet medium and environment medium is the same as the process of diffusing jet fluid.

(a) *Potential core region*: Flow within this region displays irrotational motion. Velocity gradients, either horizontal or vertical, do not exist inside of the potential core.

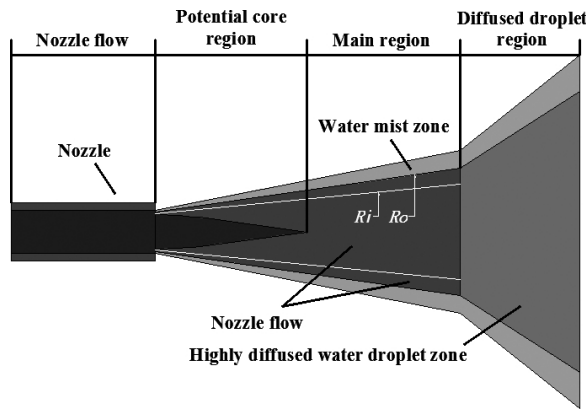


Figure 2: Jet structure based on theory and observation (Leu et al., 1998)

(b) *Main region*: Within the segment, jet axial velocity and dynamic pressure reduce gradually, and turbulence characteristics are strong. Discrepancy between the potential core region and this turbulent mixing region which is shaped by the jet medium and environment medium, fails to achieve statistical significance.

(c) *Diffused droplet region*: Jet medium and environment medium are thoroughly mixed. The jet mainly loses cohesion. Axial velocity and dynamic pressure are relatively low.

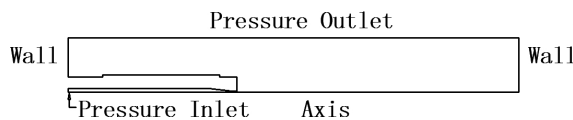


Figure 3: Computational area and boundary conditions of CC nozzle in GAMBIT

The jet in the potential core region is applied to cutting, and jetting in the diffused droplet region is applied to dust-laying and aspirating; whereas the jet in the main region, the focus of this study, is applied to cleaning and surface finish. Nozzles shown in Figure 1 widely used in engineering projects; however higher velocity, higher dynamic pressure, lower pump pressure and lower cost are necessary considerations. The optimization of nozzle structure offers a simple solution to these. The most suitable nozzle is selected for study from three kinds of nozzles, listed above.

FLUENT was used as the simulation tool. Two-dimensional simulating of the jet formation of the CC nozzle, TC nozzle and Stepped nozzle was performed first. The computational area and boundary conditions were as shown in Figure 3. The structured grid system of the nozzles was created in GAMBIT. The inlet boundary condition was a pressure inlet, and the outlet boundary condition was a pressure outlet. Water-liquid, the subject of flow in axisymmetric space, was the uncompress ideal fluid and followed a steady flow pattern.

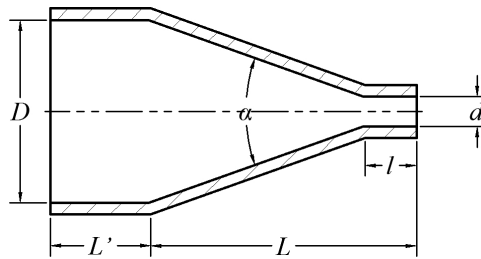


Figure 4: Main nozzle structural parameters

Figure 4 shows the main nozzle structural parameters. According to the theoretical analysis and experimental data, geometric parameters of the CC nozzle are defined $\alpha = 13^\circ$, $l/d = 3$ and $D/d = 4$. Boundary conditions were considered the inlet pressure = 100MPa, and outlet pressure of normal atmospheric pressure. The fluent fluid material was water-liquid, and the standard $k - \epsilon$ model is appropriate in our case. Nozzle outlet diameter was 0.8mm, inlet diameter 3.2mm, and computational area size $288 \times 25\text{mm}^2$ to ensure that the water jet was completely divergent. The numerical methodology expressed by Jiyuan Tu (2007) was adopted in our flow model Tu, Yeoh and Liu (2007). The flow velocity at inlet and outlet could be preliminarily roughly calculated based on the Bernoulli equation:

$$\frac{p_1}{\gamma} + \frac{v_1^2}{2g} = \frac{p_2}{\gamma} + \frac{v_2^2}{2g} \tag{1}$$

where p_1, p_2 are pressures at inlet and outlet cross-sections along the horizontal

pipeline of the nozzle, v_1 , v_2 are flow velocities at the two cross-sections, and γ denotes flow specific weight.

The equation for counting volume flux in the pipeline is then deduced:

$$q = 1.2q_0 \quad (2)$$

According to the definition $q = vA$, equation (1) is then written as follows:

$$\left(\frac{1}{2gA_1^2} - \frac{1}{2gA_2^2} \right) q_0^2 = \frac{1}{\gamma} (p_2 - p_1) \quad (3)$$

The term q_0 is a theoretical value of volume flux. Considering friction loss, more accurate volume flux q is obtained from q_0 multiplying by a friction coefficient (set to 1.2). A_1 , A_2 are areas of the two cross-sections. Certain concrete values must be used to analyze our flow model, among which A_1 as inlet cross-section area, and A_2 as outlet cross-section area, defined: $A_1 = \pi R^2$, $A_2 = \pi r^2$.

Table 1: Values of nozzle structure parameters and boundary conditions

| Parameter | Value | Unit | Note |
|-----------|-------------------|-------------------|-------|
| p_1 | 1.0×10^8 | Pa | |
| p_2 | 101325 | Pa | |
| γ | 9.81 | kN/m ³ | water |
| R | 1.6 | mm | |
| r | 0.4 | mm | |

By substituting equation (3) into (2) and adding the actual values to these equations, we obtain:

$$v_1 = 28\text{m/s};$$

$$v_2 = 447.85\text{m/s}.$$

Theoretical values v_1 and v_2 , slightly different compared to the values, are used for quantitative analysis in distinguishing flow type. One important use of the Reynolds number (Re) obtained by v_1 , regarded an essential nondimensional parameter that describes the flow characteristics, is to indicate whether the flow is turbulent or laminar. A channel flow will become turbulent if the critical Reynolds number is above 1400. Re is defined as the ratio of the *inertia force* over the *friction force*:

$$Re = \frac{\text{Inertia Force}}{\text{Friction Force}} = \frac{\rho V_1 D}{\mu}. \quad (4)$$

It is observed that the equation encapsulates three variables, density (ρ), dynamic viscosity (μ), and inlet velocity (v_1). $D(= 2R)$ is the diameter of the nozzle inlet. Combining equation (1) and (3) into (4), we obtain:

$$Re = 9.0 \times 10^4 \gg 1400$$

Thus, we confirm that the flow model is turbulent. Our case is a *constant property* fluid flow, indicating that flow density is constant, and body force in the equation can be neglected. The momentum equations employed are given as follows Leu, Meng, Geskin and Tismeneskiy (1998):

$$\frac{\partial u}{\partial t} + u \frac{\partial u}{\partial x} + v \frac{\partial u}{\partial y} = -\frac{1}{\rho} \frac{\partial p}{\partial x} + \nu \frac{\partial^2 u}{\partial x^2} + \nu \frac{\partial^2 u}{\partial y^2} \quad (5)$$

$$\frac{\partial v}{\partial t} + u \frac{\partial v}{\partial x} + v \frac{\partial v}{\partial y} = -\frac{1}{\rho} \frac{\partial p}{\partial y} + \nu \frac{\partial^2 v}{\partial x^2} + \nu \frac{\partial^2 v}{\partial y^2} \quad (6)$$

Where ν is the kinematic viscosity ($\nu = \mu/\rho$). The ν_T appeared consecutively in following equations, indicates kinematic turbulent viscosity. The nonconservative governing equations are as follows:

$$\frac{\partial u}{\partial x} + \frac{\partial v}{\partial y} = 0 \quad (7)$$

$$\begin{aligned} \frac{\partial u}{\partial t} + u \frac{\partial u}{\partial x} + v \frac{\partial u}{\partial y} &= -\frac{1}{\rho} \frac{\partial p}{\partial x} + \frac{\partial}{\partial x} \left[(\nu + \nu_T) \frac{\partial u}{\partial x} \right] + \\ \frac{\partial}{\partial y} \left[(\nu + \nu_T) \frac{\partial u}{\partial y} \right] &+ \frac{\partial}{\partial x} \left[(\nu + \nu_T) \frac{\partial u}{\partial x} \right] + \frac{\partial}{\partial y} \left[(\nu + \nu_T) \frac{\partial v}{\partial x} \right] \end{aligned} \quad (8)$$

$$\begin{aligned} \frac{\partial v}{\partial t} + u \frac{\partial v}{\partial x} + v \frac{\partial v}{\partial y} &= -\frac{1}{\rho} \frac{\partial p}{\partial y} + \frac{\partial}{\partial x} \left[(\nu + \nu_T) \frac{\partial v}{\partial x} \right] + \\ \frac{\partial}{\partial y} \left[(\nu + \nu_T) \frac{\partial v}{\partial y} \right] &+ \frac{\partial}{\partial x} \left[(\nu + \nu_T) \frac{\partial u}{\partial y} \right] + \frac{\partial}{\partial y} \left[(\nu + \nu_T) \frac{\partial v}{\partial x} \right] \end{aligned} \quad (9)$$

$$\frac{\partial T}{\partial t} + u \frac{\partial T}{\partial x} + v \frac{\partial T}{\partial y} = \frac{\partial}{\partial x} \left[\left(\frac{\nu}{Pr} + \frac{\nu_T}{Pr_T} \right) \frac{\partial T}{\partial x} \right] + \frac{\partial}{\partial y} \left[\left(\frac{\nu}{Pr} + \frac{\nu_T}{Pr_T} \right) \frac{\partial T}{\partial y} \right] \quad (10)$$

The term Pr (Prandtl number,) is defined by $Pr = \nu/\alpha$, where α denotes the molecular diffusivity of heat. Similarly, $Pr_T = \nu_T/\alpha$. In addition, the standard $k - \varepsilon$ model equations, expressed in nonconservation form, cause an increase in demand.

$$\frac{\partial k}{\partial t} + u \frac{\partial k}{\partial x} + v \frac{\partial k}{\partial y} = \frac{\partial}{\partial x} \left(\frac{\nu_T}{\sigma_k} \cdot \frac{\partial k}{\partial x} \right) + \frac{\partial}{\partial y} \left[\frac{\nu_T}{\sigma_k} \cdot \frac{\partial k}{\partial y} \right] + P - B \quad (11)$$

$$\frac{\partial \varepsilon}{\partial t} + u \frac{\partial \varepsilon}{\partial x} + v \frac{\partial \varepsilon}{\partial y} = \frac{\partial}{\partial x} \left(\frac{\nu_T}{\sigma_\varepsilon} \cdot \frac{\partial \varepsilon}{\partial x} \right) + \frac{\partial}{\partial y} \left(\frac{\nu_T}{\sigma_\varepsilon} \cdot \frac{\partial \varepsilon}{\partial y} \right) + \frac{\varepsilon}{k} (c_{\varepsilon 1} P - c_{\varepsilon 2} B) \quad (12)$$

where the destruction term B is determined by ϵ , and the production term P is formulated:

$$P = 2\nu_T \left[\left(\frac{\partial u}{\partial x} \right)^2 + \left(\frac{\partial v}{\partial y} \right)^2 \right] + \nu_T \left(\frac{\partial u}{\partial y} + \frac{\partial v}{\partial x} \right)^2. \quad (13)$$

The adjustable constants c_μ , σ_k , σ_ϵ , $c_{\epsilon 1}$ and $c_{\epsilon 2}$ are obtained by sufficient data statistics (Launder and Spalding, 1974):

$$c_\mu = 0.09, c_{\epsilon 1} = 1.44, c_{\epsilon 2} = 1.92, \sigma_k = 1.0, \sigma_\epsilon = 1.3.$$

Compared to the Stepped nozzle in Figure 5, all CC nozzle and TC nozzle demonstrate better jetting performance in the range of effective target distance. Despite that the highest velocity TC nozzle performed at the outlet, its velocity characteristic in the main region is similar to the CC nozzle. Evolved from the TC nozzle, the CC nozzle is a solid flow nozzle whose jetting behavior displays great concentrated force and stand-off-distance, where its shape proves beneficial in high precision micro-machining. To this effect, the CC nozzle was chosen as the study object in this paper. Its configuration optimization design is processed in two stages.

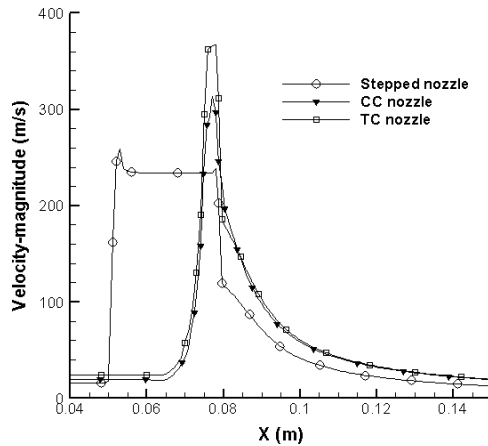


Figure 5: Three different nozzles structure comparison from simulation of jet velocity magnitude

As is commonly known, a sharp transition from the convergent section and the two cylindrical sections in the CC nozzle body would increase local resistance loss. As a solution, smooth transition of the inner surface can ensure fluid streamlining and form jetting that includes a high velocity coherent core.

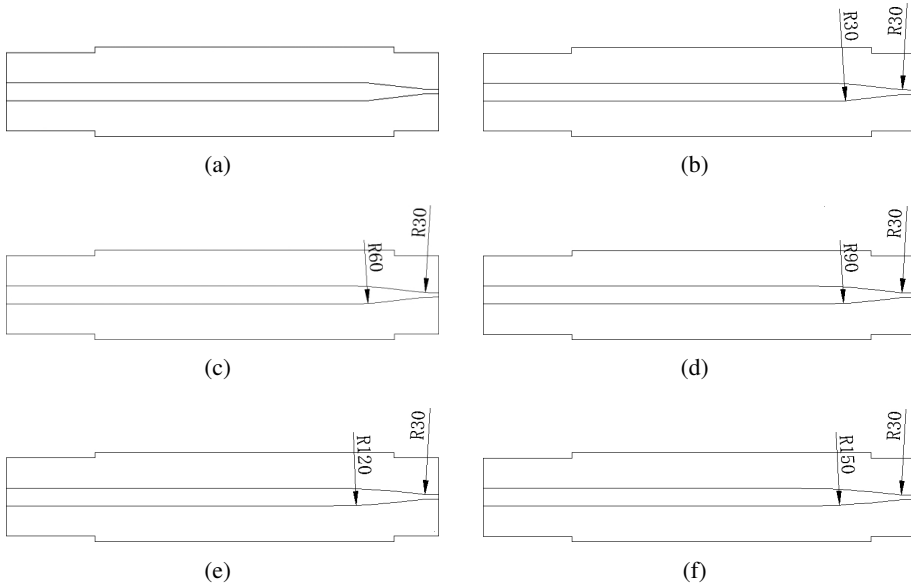


Figure 6: Preliminary structure optimization of CC nozzle

Figure 6 shows the preliminary optimization structures, in which (a) is CC nozzle, and (b)–(f) are optimized nozzles with different radii of circular arcs. These nozzles were then simulated in order to select the one with best jetting performance. According to the different nozzle structures first attempted, these nozzles were successively simulated. Velocity magnitude was chosen for simulation, as series of parameters such as velocity magnitude, axial velocity, dynamic pressure, and shooting force, all of which have positive correlation, are able to effectively measure jetting performance. As shown in Figure 7, (b) is a local display of (a) at the range of 0.078m to 0.10m in the X direction. Compared with the CC nozzle, the jetting velocity magnitude of the *R 90* nozzle is higher than others if the target distance was set in range of 0.08–0.09m. A gripping tool or manipulator installed in the high pressure water jet equipment enables the nozzle to reach any range of target distance, therefore, the *R90* nozzle is the proposed model.

3 Optimization structure of helix nozzle

To better understand the principles at work in this study, let's consider the firing of a bullet. Propelled by gunpowder, the bullet accelerates and fires through air in a rotational motion. The pressure of powder gases expels the bullet, and it continues along a predictable trajectory. As shown in Figure 8, by observing the inside of the gun barrel, the bullet expelled does not move in a straight line but a spiral at angles

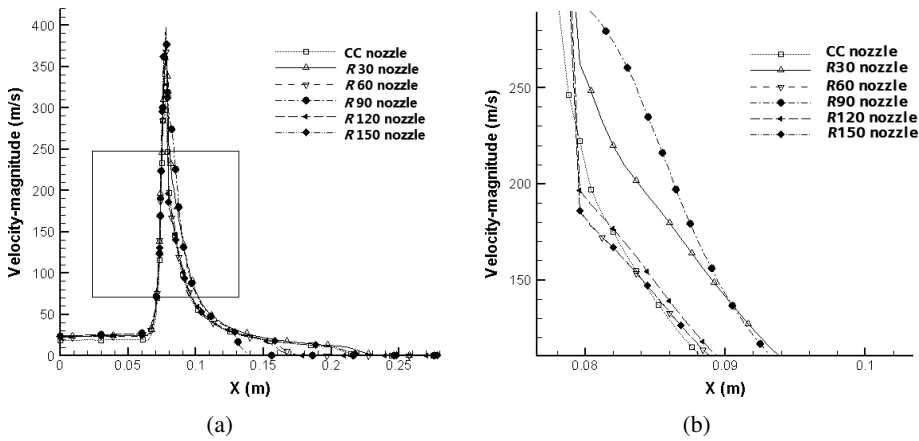


Figure 7: Jet velocity magnitude of preliminarily optimized CC nozzles compared with CC nozzle

which correspond to the centerline of the barrel. It functions similarly to a top-heavy gyroscope, in that requires a rapid spinning motion to continue its trajectory. As it flies of the barrel, the bullet must overcome air resistance. A tight spiral trajectory ensures high velocity and straight, forward shooting direction.

If we think of the flow element as a bullet, as shown in Figure 8, we can effectively structure the nozzle as a gun barrel in order to simulate rotational movement. The formation of a spiral not only guides the flow, but speeds the flow and keeps it steady. As shown in Figure 9, for precise simulation the helix nozzle, the 2D model must be transformed to 3D, as 2D cannot properly represent the complexity of a spiral. The 3D is built while keeping nozzle geometry parameters and simulating boundary conditions invariable. A structured grid system is created in the 3D model, distinguished from 2D model by two independent mesh bodies (the nozzle and computational domain), which are connected by an interface.



Figure 8: Gun barrel line structure

Observing the velocity vectors as shown in Figure 10, flow velocity magnitude apparently increases along the spiral line, and horizontal velocity almost matches the

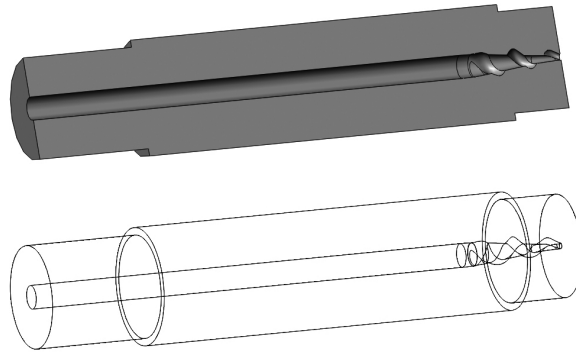


Figure 9: 3D structure of helix nozzle

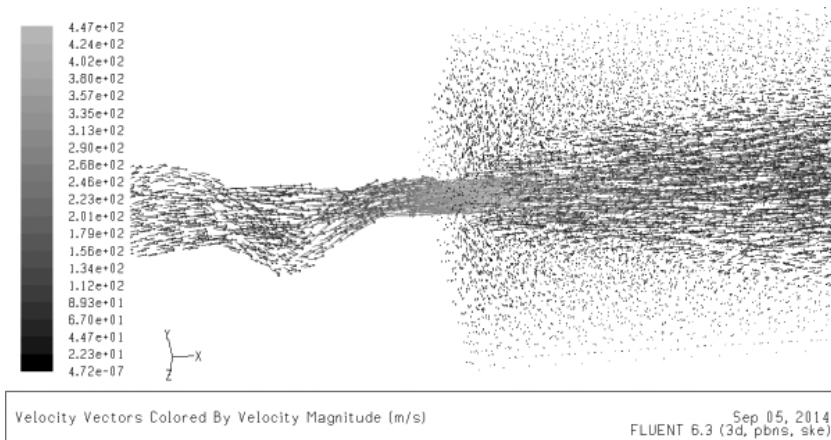


Figure 10: Velocity vectors of helix nozzle

axial velocity of the same cross section. Figure 11 shows jetting velocity magnitude along Y, and Z coordinates is not symmetrical, indicating that the high speed jet performs a shearing action on the cleaning object. In the high pressure water jet cleaning process, the jet generally loses some kinetic energy while vertically shooting at the cleaning surface. However, the jet issuing from a helix nozzle actually avoids this problem. Compared to simply changing the jetting angle, a revolving jet acts like a grinding wheel on the cleaning surface, not only displaying an impact effect but also a shearing action on the cleaning object.

As shown in Figure 12, the velocity magnitude of the helix nozzle is similar to the R90 nozzle. Disparity between the two curves is understandable considering the helix nozzle was simulated 3D and the R90 nozzle was simulated in 2D. The spiral line added to the helix nozzle's inner surface had no opposite influence on velocity.

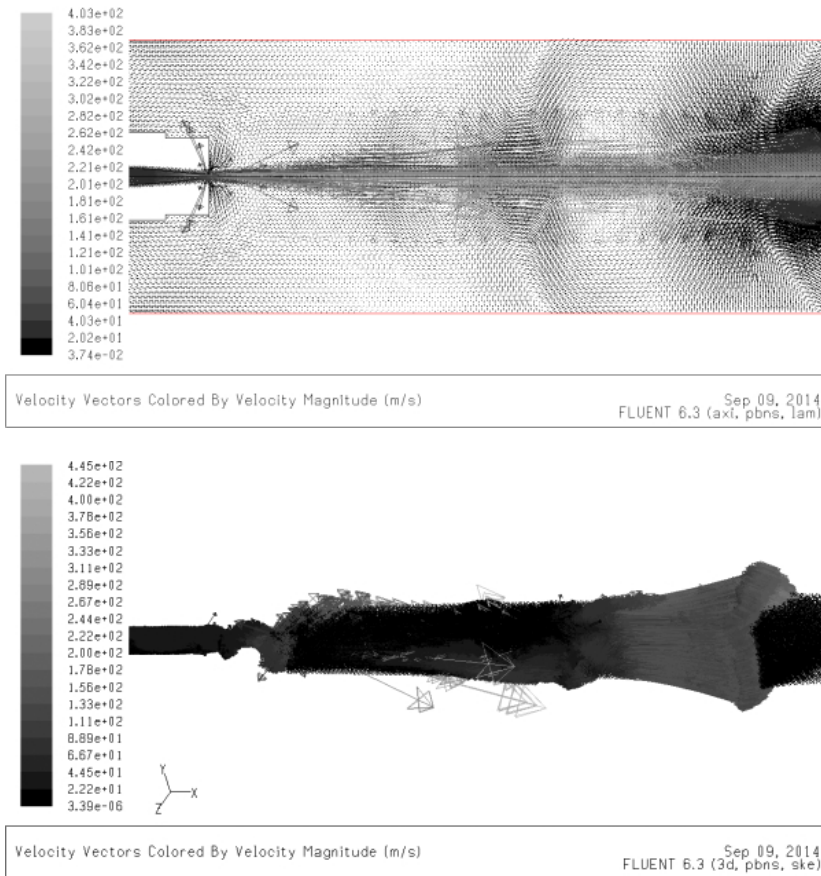


Figure 11: Contours of Velocity Vectors of *R90* nozzle and helix nozzle

Cleaning effectiveness was obvious only when the velocity value was above 150m/s. The curve denoted *R90* nozzle shows an effective cleaning range of about 0.078–0.12m (the length of nozzle in our case was 0.078m), while the effective cleaning range of the helix nozzle was about 0.078–0.143m. In a specific limit, a wider effective cleaning range produces a broader jet width, resulting in more effective cleaning.

4 Conclusion

In this paper, an effective optimization of a nozzle configuration for high pressure water jetting has been performed. The superiority and reliability of the designed object, which shows better performances in terms of dynamic pressure, cohesion, and low local resistance loss, have been also discussed to a certain extent.

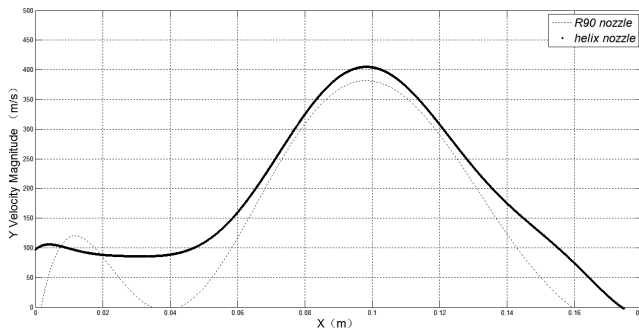


Figure 12: Velocity magnitude comparison of R90 nozzle and helix nozzle

Because the flow around the variable-area channel can dramatically change the location where particles collide and produce a whirlpool, causing local resistance loss, we have inserted a pliable structure in the nozzle's inner surface in order to increase the performances of the nozzle according to the principle of a helical accelerator.

The governing equations of turbulence proposed by Jiyuan Tu (2007) have been used to simulate the problem. At the first step of optimization, the nozzle R90 (Figure 4(d)) was chosen for subsequent experimentation. The advantages and feasibility of adding a helix to the nozzle at the outlet were confirmed by applying the rifle theory.

Future studies shall be devoted to comprehensively analyze jetting divergence phenomenon in air, considering typical aspects related to cavitation and gravity.

Funding

This work was supported by **The project of efficiently cleaning system industrialization based on robot** (grant no. 201209).

Acknowledgement: The authors acknowledge the financial support from Dalian Modern Auxiliary Machines Development and Manufacturing Co. and the purely technical help provided by Zhiyuan Jin from Dalian Polytechnic University and Pengtao Yi from Dalian Jiaotong University.

References

Gao, D.; Chen, J. (2006): Experimental research on waterjet street surface cleaning. *Proceedings of the Institution of Civil Engineers - Municipal Engineer*, vol. 159, issue 2, pp. 71-75.

Hashish, M., duPlessis, M. P.(1978): Prediction Equations Relating High Velocity Jet Cutting Performance to Stand Off Distance and Multipasses. *Journal of Manufacturing Science and Engineering*, vol. 101, issue 3, pp. 311-318

Lauder, B. E.; Spalding, D. B. (1974): The numerical computation of turbulent flows, *Computer Methods in Applied Mechanics and Engineering*, vol. 3, issue 2, pp. 269-289.

Leu, M. C.; Meng, P.; Geskin, E. S.; Tismeneskiy, L. (1998): Mathematical Modeling and Experimental Verification of Stationary Water jet Cleaning Process. *Journal of Manufacturing Science and Engineering*, vol. 120, issue 3, pp. 571-579.

Nurick, W. H. (1976): Orifice cavitation and its effect on spray mixing. *Journal of Fluids Engineering*, vol. 98, issue 4, pp. 681-687.

Soyama, H.; Yanauchi, Y., Sato, K.; Ikohagi, T.; Oba, R.; Oshima, R.(1996): High-Speed Observation of Ultrahigh-Speed Submerged Water Jets. *Experimental Thermal and Fluid Science*, vol. 12, issue 4, pp. 411-416.

Tu, J; Yeoh, G. H.; Liu, C. (2007): *Computational fluid dynamics: a practical approach*, Elsevier Science, USA.

Yanaida, K.; Ohashi, A. (1980): Flow characteristics of water jet in air. *Proceeding of 5th international symposium on jet cutting technology*, A3, pp. 33-44.

